SCIENCE CHINA
Information Sciences

• Supplementary File •

Delay-dependent stability analysis of load frequency control of microgrid based on matrix injection method

Hao-Hui FAN[1,2,3], Xing-Chen SHANGGUAN[1,2,3*], Yu-Long FAN[1,2,3],
Chuan-Ke ZHANG[1,2,3], Chen-Guang WEI[1,2,3] & Da XU[1,2,3]

[1]*School of Automation, China University of Geosciences, Wuhan 430074, China*
[2]*Hubei Key Laboratory of Advanced Control and Intelligent Automation for Complex Systems, Wuhan 430074, China*
[3]*Engineering Research Center of Intelligent Technology for Geo-Exploration, Ministry of Education, Wuhan 430074, China*

Appendix A Dynamic MG LFC Model

Firstly, the parameters to be used are listed in Table A1.

Table A1 Parameters

Parameters	Explanations
D	Damping constant of generator
K_I	Integral gain of central controller
K_P	Proportional gain of central controller
K_{il}	Integral gain of local controller
K_{pl}	Proportional gain of local controller
M	Moment of inertia of generator
R_{es}	Gain of electrolyzer system
R_{fc}	Gain of fuel cell
R_{fess}	Gain of flywheel energy storage system
R_{mt}	Drop characteristics of the micro-turbine
T_{es}	Time constant of electrolyzer system
T_{fc}	Time constant of fuel cell
T_{fess}	Time constant of flywheel energy storage system
Δf	Deviation of frequency
ΔP_{es}	Power deviation of electrolyzer system
ΔP_{fc}	Power deviation of fuel cell system
ΔP_{fess}	Power deviation of flywheel energy storage system
ΔP_{L}	Disturbance of load
ΔP_{mt}	Power deviation of micro-turbine
ΔP_{PV}	Disturbance of solar photovoltaic generation
ΔP_{WT}	Disturbance of wind turbine generation

Secondly, the model of microgrid(MG) load frequency control (LFC) shown in Fig.A1, which includes the micro-turbine (MT) with a local controller, a fuel cell (FC), an electrolyzer system (ES), a flywheel energy storage systems (FESS), the

* Corresponding author (email: star@cug.edu.cn)

central controller of the MG, and an external disturbance model. The frequency regulation involves two control loops. In the primary control loop, frequency regulation of the system involves the MT with a local controller, the FC, the ES, and the FESS. In the secondary control loop, the central controller achieves secondary frequency regulation of the system through an open communication network.

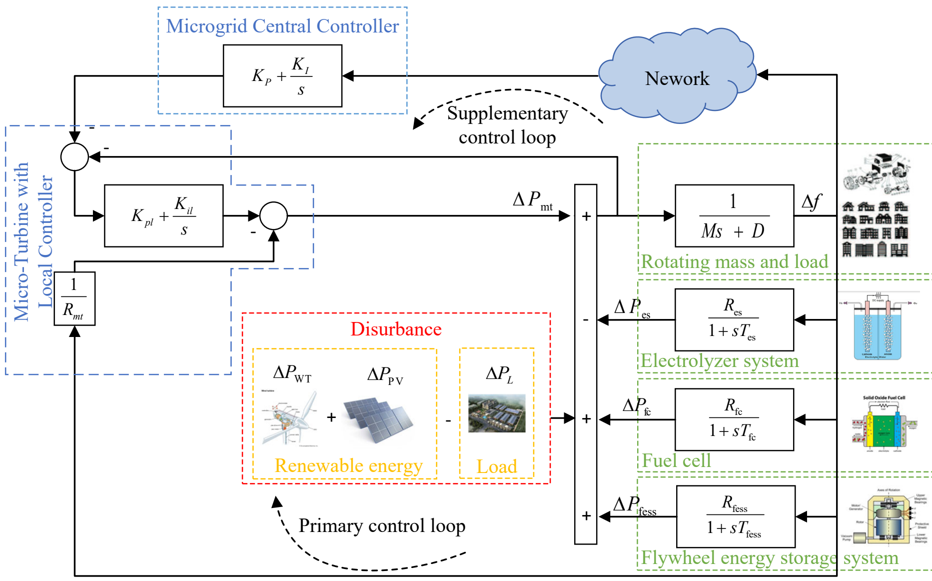

Figure A1 The frequency regulation model of MG.

Thirdly, the dynamic equation for the power deviation of the micro-turbine can be expressed as

$$\begin{aligned}\Delta\dot{P}_{\text{mt}} &= \alpha_{22}\Delta P_{\text{mt}}(t) + \alpha_{23}\Delta P_{\text{fc}}(t) + \alpha_{24}\Delta P_{\text{es}}(t) + \alpha_{25}\Delta P_{\text{fess}}(t) + \alpha_{26}\Delta f(t)\\ &\quad + \alpha_{d,21}K_I\int \Delta f(t-d(t))dt + \alpha_{d,22}\Delta P_{\text{mt}}(t-d(t)) + \alpha_{d,23}\Delta P_{\text{fc}}(t-d(t))\\ &\quad + \alpha_{d,24}\Delta P_{\text{es}}(t-d(t)) + \alpha_{d,25}\Delta P_{\text{fess}}(t-d(t)) + \alpha_{d,26}\Delta f(t-d(t))\\ &\quad - \alpha K_{pl}\Delta\dot{P}_{\text{dis}}(t) - \alpha K_{il}\Delta P_{\text{dis}}(t),\end{aligned} \tag{A1}$$

where

$$\begin{aligned}&\alpha = \frac{1}{1+K_{pl}}, \alpha_{22} = \alpha(-K_{il} - \frac{1}{MR_{mt}}), \alpha_{23} = \alpha(\frac{K_{pl}}{T_{\text{fc}}} - K_{il} - \frac{1}{MR_{mt}}),\\ &\alpha_{24} = \alpha(-\frac{K_{pl}}{T_{\text{es}}} + K_{il} + \frac{1}{MR_{mt}}), \alpha_{25} = \alpha(\frac{K_{pl}}{T_{\text{fess}}} - K_{il} - \frac{1}{MR_{mt}}),\\ &\alpha_{26} = \alpha(-\frac{K_{pl}R_{\text{fc}}}{T_{\text{fc}}} + \frac{K_{pl}R_{\text{es}}}{T_{\text{es}}} + \frac{D}{MK_{\text{mt}}}), \alpha_{d,21} = -\alpha K_{il},\\ &\alpha_{d,22} = \alpha_{d,23} = -\alpha_{d,24} = \alpha_{d,25} = -\alpha\frac{K_P K_{pl}}{M},\\ &\alpha_{d,26} = \alpha(-\frac{K_{pl}R_{\text{fc}}}{T_{\text{fc}}} + \frac{K_{pl}R_{\text{es}}}{T_{\text{es}}} + \frac{D}{MK_{\text{mt}}}).\end{aligned}$$

Appendix B Proof and discussion of Theorem 1

The part gives the detailed proof of the following Theorem 1. The standard notations to be used are listed in Table B1.

Theorem 1. For given scalars d_i, $i = 1,2$, system (1) is asymptotically stable if there exist $P = \{P_{ij}\}_{5\times 5} \in \mathbb{S}_+^{5n}, \{Q, R_i\} \in \mathbb{S}_+^n$, $i = 1,2$, $Z = \{Z_{ij}\}_{4\times 4} \in \mathbb{S}_+^{4n}$, any matrices $\{L_1, N_1\} \in \mathbb{R}^{3n\times 10n}$, $\{L_2, N_2\} \in \mathbb{R}^{3n\times 2n}, S_1 \in \mathbb{R}^{2n\times 2n}$, and $S_2 \in \mathbb{R}^{2n\times 10n}$ such that the following inequalities holds for $d \in \{d_1, d_2\}$.

$$\begin{bmatrix}\Psi_1 & S_2^{\mathrm{T}} - d(E_A^{\mathrm{T}}S_1 - E_B^{\mathrm{T}}\Phi_2^{\mathrm{T}}) & d_{1d}N_1^{\mathrm{T}} + d_{2d}L_1^{\mathrm{T}}\\ * & d\Phi_1 + \mathrm{He}\{S_1\} & d_{1d}N_1^{\mathrm{T}} + d_{2d}L_2^{\mathrm{T}}\\ * & * & -d_{12}^2\hat{R}_2\end{bmatrix} < 0, \tag{B1}$$

where

$e_i = [0_{n\times(i-1)n}, I_n, 0_{n\times(10-i)n}], i = 1,2,\ldots,10$

$e_s = Ae_1 + A_d e_3, e_0 = 0_{n\times 10n}$,
$E_i = [e_i^{\mathrm{T}} - e_{i+1}^{\mathrm{T}}, e_i^{\mathrm{T}} + e_{i+1}^{\mathrm{T}} - 2e_{i+4}^{\mathrm{T}}, e_i^{\mathrm{T}} - e_{i+1}^{\mathrm{T}} + 6e_{i+4}^{\mathrm{T}} - 12e_{i+7}^{\mathrm{T}}]^{\mathrm{T}}, i = 1, 2, 3$
$e_a = d_{1d}^2 e_9 + d_{2d}^2 e_{10} + d_{2d} d_{1d} e_6, e_b = (d_1 + d_2)e_6 - 2d_1 e_9 - 2d_2 e_{10}$,
$\Pi_1 = [e_1^{\mathrm{T}}, d_1 e_5^{\mathrm{T}}, d_{1d} e_6^{\mathrm{T}} + d_{2d} e_7^{\mathrm{T}}, d_1^2 e_8^{\mathrm{T}}, e_a^{\mathrm{T}}]^{\mathrm{T}}$,
$\Pi_2 = [e_s^{\mathrm{T}}, e_1^{\mathrm{T}} - e_2^{\mathrm{T}}, e_2^{\mathrm{T}} - e_4^{\mathrm{T}}, d_1(e_1^{\mathrm{T}} - e_5^{\mathrm{T}}), d_{12} e_2^{\mathrm{T}} - d_{1d} e_6^{\mathrm{T}} - d_{2d} e_7^{\mathrm{T}}]^{\mathrm{T}}$,
$\Pi_3 = [e_2^{\mathrm{T}}, e_1^{\mathrm{T}}, e_0^{\mathrm{T}}, d_{1d} e_6^{\mathrm{T}} + d_{2d} e_7^{\mathrm{T}}]^{\mathrm{T}}, \Pi_4 = [e_4^{\mathrm{T}}, e_1^{\mathrm{T}}, d_{1d} e_6^{\mathrm{T}} + d_{2d} e_7^{\mathrm{T}}, e_0^{\mathrm{T}}]^{\mathrm{T}}$,
$\Pi_5 = [e_0^{\mathrm{T}}, e_s^{\mathrm{T}}, e_2^{\mathrm{T}}, -e_4^{\mathrm{T}}]^{\mathrm{T}}$,
$\Pi_6 = [d_{1d} e_6^{\mathrm{T}} + d_{2d} e_7^{\mathrm{T}}, d_{12} e_1^{\mathrm{T}}, e_a^{\mathrm{T}}, d_{12}(d_{1d} e_6^{\mathrm{T}} + d_{2d} e_7^{\mathrm{T}}) - e_a^{\mathrm{T}}]^{\mathrm{T}}$,
$E_A = [e_9^{\mathrm{T}} + e_{10}^{\mathrm{T}} - e_6^{\mathrm{T}}, e_7^{\mathrm{T}} - e_6^{\mathrm{T}}]^{\mathrm{T}}, E_B = [e_7^{\mathrm{T}} - e_6^{\mathrm{T}}, e_b^{\mathrm{T}}, \Pi_{2|d=0}^{\mathrm{T}}, \Pi_5^{\mathrm{T}}]^{\mathrm{T}}$,
$\hat{R}_i = \mathrm{diag}\{R_i, 3R_i, 5R_i\}, i = 1, 2$
$\Upsilon_1 = \mathrm{He}\{\Pi_1^{\mathrm{T}} P \Pi_2\} + e_1^{\mathrm{T}} Q e_1 - e_2^{\mathrm{T}} Q e_2$,
$\Upsilon_2 = \Pi_3^{\mathrm{T}} Z \Pi_3 - \Pi_4^{\mathrm{T}} Z \Pi_4 + \mathrm{He}\{\Pi_5^{\mathrm{T}} Z \Pi_6\}$,
$\Upsilon_3 = e_s^{\mathrm{T}}(d_1^2 R_1 + d_{12}^2 R_2)e_s - E_1^{\mathrm{T}} \hat{R}_1 E_1$,
$P_5 = [0_n, 0_n, 0_n, 0_n, I_n] \times P$,
$P_{5i} = P_5 \times [0_{n\times(i-1)n}, I_n, 0_{n\times(5-i)n}]^{\mathrm{T}}, i = 3, 5$
$Z_i = [0_{n\times(i-1)n}, I_n, 0_{n\times(4-i)n}] \times Z, i = 3, 4$
$Z_{ii} = Z_i \times [0_{n\times(i-1)n}, I_n, 0_{n\times(4-i)n}]^{\mathrm{T}}, i = 3, 4$
$\Phi_1 = \begin{bmatrix} 0_n & P_{55} \\ * & 0_n \end{bmatrix}, \Phi_2 = \begin{bmatrix} 0_n & 0_n & P_5 & Z_3 - Z_4 \\ \frac{Z_{44} - Z_{33}}{2} - P_{53} & P_{55} & 0_{n\times 5n} & 0_{n\times 4n} \end{bmatrix}$,
$\Theta_{11} = -\mathrm{He}\left\{ dE_A^{\mathrm{T}} S_2 + \begin{bmatrix} E_2 \\ E_3 \end{bmatrix}^{\mathrm{T}} \begin{bmatrix} N_1 + dN_2 E_A \\ L_1 + dL_2 E_A \end{bmatrix} \right\}$,
$\Psi_1 = \Upsilon_1 + \Upsilon_2 + \Upsilon_3 + \Theta_{11} - d^3 E_A \Phi_1 E_A - d^2 \mathrm{He}\{E_A^{\mathrm{T}} \Phi_2 E_B\}$.

Table B1 Notations

Notations	Explanations
$\mathbb{R}^n$	The sets of n-dimensional vectors
$\mathbb{R}^{m\times n}$	The sets of $m \times n$-dimensional real matrices
$\mathbb{S}_+^{n\times n}$	The sets of $n \times n$-dimensional symmetric positive definite matrices
$X > 0\ (\geqslant 0)$	Symmetric and positive-definite (semi-positive-definite) matrix, X
X^{T}	The transpose of matrix X
X^{-1}	The inverse of matrix X
$\mathrm{col}\{\cdots\}$	The block-diagonal matrixes
$\mathrm{He}\{X\}$	$X + X^{\mathrm{T}}$
$\mathrm{diag}\{\cdots\}$	The block-diagonal matrixes

Proof. To simplify the representation of Lemma 1, the following condition is given:

$$\mathcal{F}_3(d) = \eta^{\mathrm{T}} \left(d^3 \Gamma_1^{\mathrm{T}} \Xi_1 \Gamma_1 + d^2 \mathrm{He}\{\Gamma_1^{\mathrm{T}} \Xi_2 \Gamma_2\} + \Xi_3 + \frac{\Gamma_3^{\mathrm{T}} \Xi_4 \Gamma_3}{d_{1d}} + \frac{\Gamma_4^{\mathrm{T}} \Xi_5 \Gamma_4}{d_{2d}} \right) \eta, \tag{B2}$$

where $\Gamma_1 \in \mathbb{R}^{p\times m}, \Gamma_2 \in \mathbb{R}^{l\times m}, \Gamma_3 \in \mathbb{R}^{q\times m}, \Gamma_4 \in \mathbb{R}^{r\times m}$. $\Xi_1 \in \mathbb{S}^p, \Xi_2 \in \mathbb{R}^{p\times l}, \Xi_3 = d\Omega_{p1} + \Omega_{p0} \in \mathbb{S}^m$ is convex with respect to $\Xi_4 \in \mathbb{S}^q,\ \Xi_5 \in \mathbb{S}^r;\ \{p, q, r, l, m\} \in \mathbb{N}$, and $p < m,\ q < m,\ r < m$. $\Omega_{pi} \in \mathbb{S}^m,\ i = 0, 1$.

Lemma 1: ([3]). Consider $\mathcal{F}_3(d)$ defined in (B2). $\mathcal{F}_3(d) \leqslant 0$ satisfies for all $d \in \{d_1, d_2\}$, if there exists $L_1 \in \mathbb{R}^{r\times m}$, $L_2 \in \mathbb{R}^{r\times p}$, $N_1 \in \mathbb{R}^{q\times m}$, $N_2 \in \mathbb{R}^{q\times p}$, $S_1 \in \mathbb{R}^{p\times p}$, and $S_2 \in \mathbb{R}^{p\times m}$, such that the following holds.

$$\mathcal{G}(d) = \begin{bmatrix} \Xi_3 + \Theta_{11} & d\Gamma_2^{\mathrm{T}} \Xi_2^{\mathrm{T}} + \Theta_{12} & d_{1d} N_1^{\mathrm{T}} + d_{2d} L_1^{\mathrm{T}} \\ * & d\Xi_1 + \mathrm{He}\{S_1\} & d_{1d} N_2^{\mathrm{T}} + d_{2d} L_2^{\mathrm{T}} \\ * & * & d_{1d} \Xi_4 + d_{2d} \Xi_5 \end{bmatrix} < 0, \tag{B3}$$

where

$$\Theta_{11} = -\mathrm{He}\left\{ d\Gamma_1^{\mathrm{T}} S_2 + \begin{bmatrix} \Gamma_3 \\ \Gamma_4 \end{bmatrix}^{\mathrm{T}} \begin{bmatrix} N_1 + dN_2\Gamma_1 \\ L_1 + dL_2\Gamma_1 \end{bmatrix} \right\}, \Theta_{12} = S_2^{\mathrm{T}} - d\Gamma_1^{\mathrm{T}} S_1.$$

For ease of reading, the following vectors are defined:

$$\begin{aligned}
\xi(t) =& \mathrm{col}\Bigg\{ x(t), x(t-d_1), x(t-d), x(t-d_2), \int_{t-d_1}^{t} \frac{x(s)}{d_1}\, ds, \int_{t-d}^{t-d_1} \frac{x(s)}{d_{1d}}\, ds, \int_{t-d_2}^{t-d} \frac{x(s)}{d_{2d}}\, ds, \\
& \int_{t-d_1}^{t}\int_{\theta}^{t} \frac{x(s)}{d_1^2}\, ds\, d\theta, \int_{t-d}^{t-d_1}\int_{\theta}^{t-d_1} \frac{x(s)}{d_{1d}^2}\, ds\, d\theta, \int_{t-d_2}^{t-d}\int_{\theta}^{t-d} \frac{x(s)}{d_{2d}^2}\, ds\, d\theta \Bigg\}, \\
\varsigma_1(t) =& \mathrm{col}\left\{ x(t), \int_{t-d_1}^{t} x(s)\, ds, \int_{t-d_1}^{t-d_2} x(s)\, ds, \int_{-d_1}^{0}\int_{t+\theta}^{t} x(s)\, ds\, d\theta, \int_{-d_1}^{-d_2}\int_{t+\theta}^{t-d_1} x(s)\, ds\, d\theta \right\}, \\
\varsigma_2(t) =& \mathrm{col}\left\{ x(s), x(t), \int_{s}^{t-d_1} x(u)\, du, \int_{t-d_2}^{s} x(u)\, du \right\}.
\end{aligned}$$

Consider the following Lyapunov-Krasovskii functional (LKF) candidate:

$$V(t) = V_1(t, x_t) + V_2(t, x_t) + V_3(t, \dot{x}_t), \tag{B4}$$

where

$$\begin{aligned}
V_1(t, x_t) &= \varsigma_1^{\mathrm{T}}(t) P \varsigma_1(t), \\
V_2(t, x_t) &= \int_{t-d_1}^{t} x^{\mathrm{T}}(s) Q x(s) ds + \int_{t-d_2}^{t-d_1} \varsigma_2^{\mathrm{T}}(t,s) Z \varsigma_2(t,s)\, ds, \\
V_3(t, \dot{x}_t) &= \sum_{i=1}^{2} (d_i - d_{i-1}) \int_{-d_i}^{-d_{i-1}} \int_{t+\theta}^{t} \dot{x}^{\mathrm{T}}(s) R_i \dot{x}(s) ds d\theta.
\end{aligned}$$

with calculating the derivative of the $V(t)$, the following inequality can be obtained:

$$\begin{aligned}
\dot{V}(t) &= \dot{V}_1(t, x_t) + \dot{V}_2(t, x_t) + \dot{V}_3(t, \dot{x}_t) \\
&\leqslant \xi^{\mathrm{T}}(t) \left(\sum_{i=1}^{3} \Upsilon_i - J_1 - J_2 \right) \xi(t),
\end{aligned} \tag{B5}$$

where

$$\begin{aligned}
J_1 &= d_1 \int_{t-d_1}^{t} \dot{x}^{\mathrm{T}}(s) R_1 \dot{x}(s)\, ds, \\
J_2 &= d_{12} \int_{t-d}^{t-d_1} \dot{x}^{\mathrm{T}}(s) R_2 \dot{x}(s)\, ds + d_{12} \int_{t-d_2}^{t-d} \dot{x}^{\mathrm{T}}(s) R_2 \dot{x}(s)\, ds.
\end{aligned}$$

which are estimated, based on auxiliary function-based integral inequalities [4], as,

$$J_1 \geqslant \xi^{\mathrm{T}}(t) E_1^{\mathrm{T}} \hat{R}_1 E_1 \xi(t), \tag{B6}$$

$$J_2 \geqslant \xi^{\mathrm{T}}(t) \left(\frac{d_{12} E_2^{\mathrm{T}} \hat{R}_2 E_2}{d_{1d}} + \frac{d_{12} E_3^{\mathrm{T}} \hat{R}_2 E_3}{d_{2d}} \right) \xi(t). \tag{B7}$$

Combining (B1), (B4) and (B5), the following inequality can be obtained:

$$\dot{V}(t) \leqslant \xi^{\mathrm{T}}(t) \Omega(d) \xi(t), \tag{B8}$$

with

$$\Omega(d) = \Upsilon_1 + \Upsilon_2 + \Upsilon_3 - \frac{d_{12} E_2^{\mathrm{T}} \hat{R}_2 E_2}{d_{1d}} - \frac{d_{12} E_3^{\mathrm{T}} \hat{R}_2 E_3}{d_{2d}}.$$

It can be found that the non-convex terms (d^3-and d^2-dependent terms) only appear in $\mathrm{He}\{\Pi_1^{\mathrm{T}} P \Pi_2\}$ of Υ_1 and Υ_2. These terms are nonlinear with respect to d and need to be subtracted in Ψ_1. After simple mathematical calculations, (B8) can be rewritten as the form of (B2) with $\eta = \xi(t)$ and

$$\begin{Bmatrix}
\Gamma_1 = E_A \in \mathbb{R}^{2n \times 10n}, & \Gamma_3 = E_2 \in \mathbb{R}^{3n \times 10n} \\
\Gamma_2 = E_B \in \mathbb{R}^{11n \times 10n}, & \Gamma_4 = E_3 \in \mathbb{R}^{3n \times 10n} \\
\Xi_1 = \Phi_1 \in \mathbb{S}^{2n}, & \Xi_3 = \Upsilon(d) = \Psi_1 - \Theta_{11} \in \mathbb{S}^{10n} \\
\Xi_2 = \Phi_2 \in \mathbb{R}^{2n \times 11n}, & \Xi_i = -d_{12} \hat{R}_2 \in \mathbb{S}^{3n},\ i = 4, 5
\end{Bmatrix}. \tag{B9}$$

Thus, for any $\{L_1, N_1\} \in \mathbb{R}^{3n \times 10n}$, $\{L_2, N_2\} \in \mathbb{R}^{3n \times 2n}$, $S_1 \in \mathbb{R}^{2n \times 2n}$ and $S_2 \in \mathbb{R}^{2n \times 10n}$, applying Lemma 1 shows that if LMI (B1) holds for $d \in \{d_1, d_2\}$, then $\Omega(d) < 0$ holds for all $d(t) \in [d_1, d_2]$, which further implies $\dot{V}(t) \leqslant -\epsilon \|x(t)\|^2$ for a sufficiently small $\epsilon > 0$.

If $P > 0, Q > 0, Z > 0, R_i > 0,\ i = 1,\ 2$ and LMI (B1) hold, system (1) is stable, completing the proof.

Appendix C CASE STUDIES

To verify the accuracy of the calculated delay stability margin, specifically the gap between the calculated and actual maximum tolerable delay, and thus demonstrate the effectiveness of the method proposed in this paper, relevant simulation analyses are conducted using MATLAB's Simulink platform.

Assume the system experiences a disturbance of 0.01 p.u. at $t = 10s$ with controller gains of $K_P = 5$ and $K_I = 0.2$. The frequency responses corresponding to the delay margins t_2 (calculated using the method introduced in this paper), t_3 (from [1]), and t_1 representing the critical maximum delay found through simulation are shown in Fig. C1.

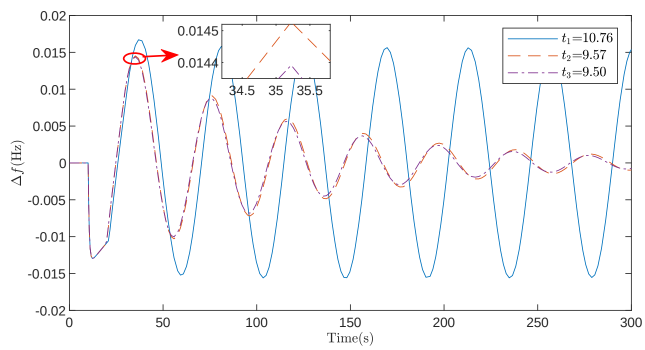

Figure C1 Frequency deviation response curves under different delay conditions.

In order to simulate the random changes in the time delay of a real MG, 200 randomly selected scenarios are generated. The controller gains are configured as $K_P = 5$ and $K_I = 0.2$, and the time delay randomly chosen from the range $[0, 9.57]$. Fig. C2 shows the results of two hundred simulations with initial conditions $\Delta f \in [-0.02, 0.02]$ to validate the effectiveness of the proposed method. The results demonstrate that the MG maintains asymptotic stability despite the presence of time delay.

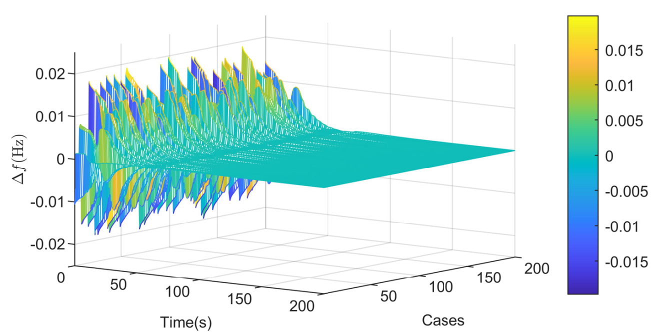

Figure C2 Frequency deviation under 200 simulation results.

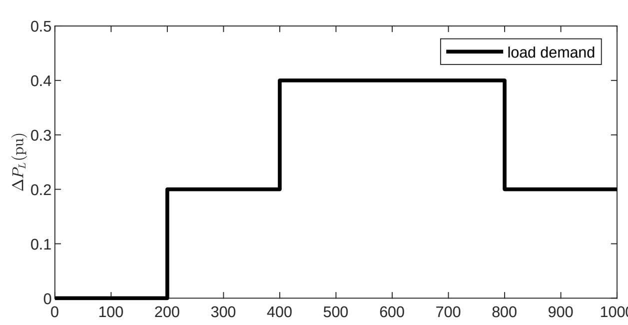

Figure C3 Actual load variation.

To simulate the frequency response of a time-delay MG in an actual power environment, load demand (Fig. C3) and renewable energy sources (RESs) power fluctuations [2] (Fig. C4) are applied to the system. The MG controller gains are set to $K_P = 5$ and $K_I = 0.2$, and the time delay is chosen randomly from the range $[0, 9.57]$. To observe peak frequency

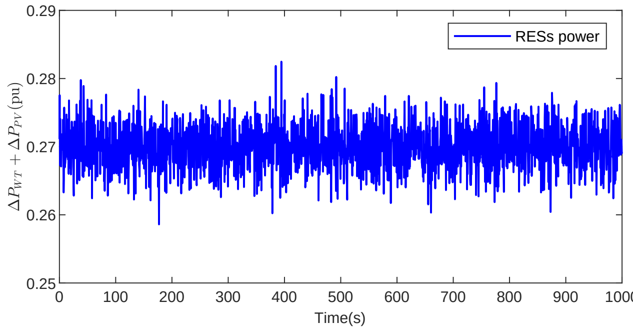

Figure C4 RESs power fluctuations.

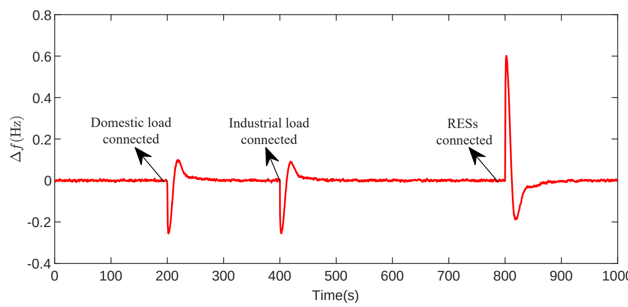

Figure C5 Frequency response curves under load fluctuations and RESs permeation.

fluctuations, a 0.2 p.u. domestic load is connected at 200s, and a 0.2 p.u. industrial load is connected at 400s and RESs is connected at 800s. According to the results of Fig. C5, the system maintains a frequency deviation within ± 0.01 Hz during normal operation. A dip of 0.256 Hz occurs when the domestic load is connected at 200s, and a dip of 0.254 Hz occurs when the industrial load is connected at 400s. At 800s, an overshoot of 0.601 Hz occurs when the RESs are connected. These results indicate that the system remains stable despite the influence of time delay in an actual power environment.

References

1 Wei C G, Shangguan X C, He Y, et al. Delay-dependent stability evaluation for temperature control load participating in load frequency control of microgrid. IEEE Transactions on Industrial Electronics, 2025, 72: 449-459.

2 Saxena P, Singh N, Ashok K P. Enhancing the transient performance and dynamic stability of microgrid using PI inertia injection controller. International Journal of Electrical Power and Energy Systems, 2022, 134: 107334.

3 Fan Y L, Zhang C K, Liu Y F, et al. Stability analysis of systems with time-varying delays for conservatism and complexity reduction. Systems and Control Letters, 2024, 193: 105948.

4 Park P, Lee W I, Lee S Y. Auxiliary function-based integral inequalities for quadratic functions and their applications to time-delay systems. Journal of the Franklin Institute, 2015, 352: 1378-1396.